Local Nucleon-Nucleon Potentials Based upon Chiral Effective Field Theory

Presented in Partial Fulfillment of
the Requirements for the Degree of

Master of Science

with a

Major in Physics

in the

College of Graduate Studies

University of Idaho

by

Philip Herd

Major Professor
Ruprecht Machleidt, Ph.D.

Committee
Francesca Sammarruca, Ph.D.
Matthew M. Hedman, Ph.D.

Department Administrator
Ray von Wandruszka, Ph.D.

December 2015

AUTHORIZATION TO SUBMIT THESIS

This thesis of Philip Herd, submitted for the degree of Master of Science with a Major in Physics and titled "Local Nucleon-Nucleon Potentials based upon Chiral Effective Field Theory," has been reviewed in final form. Permission, as indicated by the signatures and dates below, is now granted to submit final copies to the College of Graduate Studies for approval.

Major Professor:	Ruprecht Machleidt, Ph. D.	Date
Committee Members:	Francesca Sammarruca, Ph. D.	Date
	Matthew M. Hedman, Ph. D.	Date
Department Chair:	Ray von Wandruszka, Ph. D.	Date

ABSTRACT

During the past three decades, it has been demonstrated that chiral effective field theory (EFT) represents a powerful tool to deal with hadronic interactions at low energy in a systematic and model-independent way. Within the last decade, precision nucleon-nucleon (NN) potentials based upon chiral EFT have been constructed. Most of these potentials have been represented in momentum-space. However, there are some important applications in nuclear physics for which a representation of the NN potential in position space is preferred. Therefore, in this thesis, a NN potential is constructed that is local and given in position space in a relatively simple form. In terms of the chiral expansion, we advance to next-to-next-to-leading order and achieve accuracy that is superior to similar potentials constructed by other researchers. Our potential will serve as an excellent starting point for ab initio few- and many- body calculations in nuclear physics.

ACKNOWLEDGEMENTS

I would like to thank Dr. Ruprecht Machleidt for his immense support and help during my career here at the University of Idaho.

Table of Contents

List of Tables

LIST OF FIGURES

CHAPTER 1

INTRODUCTION

In 1911 Rutherford discovered the atomic nucleus by showing that a positively charged core with a small radius can describe alpha particle scattering at large angles [1]. Soon after, Thomson discovered isotopes from studying nuclear masses [2]. The first nuclear models developed at this time used electrostatic forces with protons and electrons to build nuclei. However, this raised questions of how a nucleus could stay together [3]. The neutron was then discovered by Chadwick in 1932 [4]. This implied that both the neutron and proton were the basic components of a nucleus. Because of this, a new force had to be considered to bind the nucleus together. This force is called both the Strong Force and the Nuclear Force.

Soon after, Wigner concluded from studying the binding energies of light nuclei [5] that the force was strong within a short range. Theoretical ideas were proposed by Majorana [6] and Heisenberg [7] to explain how the nucleus can reach saturation. Heisenberg also suggested that both the proton and neutron could be two different states of one particle. Meanwhile, proton-proton scattering experiments up to 1 MeV were conducted [8] and the deuteron's binding energy was measured [9]. Since then, various theories have come about to describe this force.

In 1935, Yukawa was the first to create a fundamental explanation for the nuclear force [10]. He did so by assuming that the nucleons interact by exchanging massive scalar particles later called mesons. Doing this creates a potential which is proportional to $\frac{1}{r}e^{-\mu r}$ where r is the distance between the nucleons and μ is the mass of the

meson. The theory was soon extended. Proca [11] and Kemmer [12] added pseudo-scalar and -vector particles. Later, Schwinger [13], Møller and Rosenfeld [14] derived the quadrupole moment for the deuteron. A pseudo-scalar meson was predicted in 1946 [15] and found the following year [16]. This particle is called the π-meson or pion.

In 1951, Taketani, Nakamura and Sasaki suggested dividing the nuclear force was divided into three regions [17] consisting of a short range ($r < 1$ fm), an intermediate range (1 fm $< r <$ 2 fm) and a long range ($r >$ 2 fm). A potential was derived from an expansion in terms of the particle number [18], but the pair terms had to be dropped [19] to match experimental data. Later, chiral symmetry was conceived [20, 21, 22] to explain the pair suppression. In the 1970's, dispersion relations [23, 24] and field theoretical approaches [25, 26] were pursued to further develop meson theory. One of the most elaborate models was developed by the Bonn group. Multi-pion exchange diagrams were calculated and the final result accurately agrees with the nucleon - nucleon scattering data [27].

Even though this meson theory works quite well in explaining the experimental data, there are issues. Mesons are not fundamental particles; the models require a fictitious σ-meson [27] (which may or may not exist); and mesons are roughly the size of a proton if they are viewed as hard spheres - meaning that they can't fit between nucleons in the nucleus.

The fundamental theory of strong interaction is quantum chromodynamics (QCD). It uses quarks and gluons to build both mesons and nucleons. A six quark model has

been made for the deuteron which matches up to its quantum numbers and explains multiple features of low energy nuclear physics [28].

At low energies, QCD is non-perturbative. Because of this, QCD has been approximated and simplified into an effective field theory (EFT) [29]. Using pions and nucleons as the effective degrees of freedom, the most general Lagrangian which observes the broken chiral symmetry of QCD can be written down. This approach has become known as chiral effective field theory.

This thesis constructs an NN potential based on the above theory in position space, also known as configuration or r space. NN potentials have been constructed before [30, 31] but mainly in momentum space. However, some microscopic nuclear structure calculations, such as the ground state of light nuclei ($A \leq 40$), are more conveniently performed in position space. It is therefore the purpose of this thesis to provide a local position space NN potential.

CHAPTER 2

EFFECTIVE FIELD THEORY

2.1 POWER COUNTING

At low energies, QCD is non-perturbative. As such, the structure and dynamics of hadrons can't be determined analytically. This is where EFT comes in as it shows how to calculate hadronic interactions at low energies. This is based on work by Weinberg [29] which involves writing down the most general Lagrangian and calculating the matrix elements to the given order. This was the starting point for chiral effective field theory.

In order to determine which Feynman diagrams should be kept in the terms of the expansion up to a given order, Weinburg's power counting is used. The counting is done in terms of $(Q/\Lambda_\chi)^\nu$ where Q stands for a momentum or pion mass and $\Lambda_\chi (\approx 1\,\mathrm{GeV})$ is the chiral symmetry breaking scale [32]. The power ν of a diagram is given by:

$$\nu = -2 + 2A - 2C + 2L + \sum_i \Delta_i \tag{2.1}$$

with

$$\Delta_i = d_i + \frac{n_i}{2} - 2\,, \tag{2.2}$$

where A is the number of nucleons, C is the number of separately connected pieces, L is the number of loops in the related diagram, d_i is the number of derivatives or pion-mass insertions and n_i is the number of nucleon fields involved with vertex i. Δ_i is called the index of the vertex. See Ref. [33] for a derivation.

Figure 2.1 shows the counting scheme and its related Feynman diagrams [32]. LO (Leading Order, $\nu = 0$) describes the two nucleon force to a rough approximation: just the one-pion exchange (1PE) and contact terms that contribute only to the S-waves. $\nu = 1$ does not exist because it violates time-reversal and parity invariances. NLO (Next-to-Leading Order, $\nu = 2$) describes the two nucleon force to a better degree by including more contact terms as well as the two-pion exchange (2PE) in several ways it can occur. Finally, at N^{2}LO (Next-to-Next-to-Leading Order, $\nu = 3$), a realistic 2PE emerges [32].

2.2 THE LAGRANGIANS

For pion-pion ($\pi\pi$) scattering, the Lagrangian (up to $\nu = 4$) is given by

$$\mathcal{L}_{\pi\pi}^{(\nu=2)} = \frac{1}{2}\partial_\mu\vec{\pi}\partial^\mu\vec{\pi} + \frac{1}{6f_\pi^2}\left[\left(\vec{\pi}\partial_\mu\vec{\pi}\right)^2 - \vec{\pi}^2\left(\partial_\mu\vec{\pi}\partial^\mu\vec{\pi}\right)\right] - \frac{m_\pi^2}{2}\vec{\pi}^2 + \frac{m_\pi^2}{24f_\pi^2}\vec{\pi}^4, \qquad (2.3)$$

where $\vec{\pi}$ denotes the pion fields and m_π is the pion mass. f_π is the pion decay constant. The predictions for $\pi\pi$ scattering are consistent with the experimental data.

For meson-nucleon scattering (πN), some items must be considered in order to keep the power counting method mentioned above. As the nucleon is much more massive than the pion, the nucleon needs to be modelled as a static physical object to prevent a violation of the chiral limit [34]. This approach is called heavy baryon chiral perturbation theory. Within this framework, the Lagrangians read [35]

$$\mathcal{L}_{\pi N}^{(\nu=1)} = \bar{N}(iD_0 - \frac{g_A}{2}\vec{\sigma}\cdot\vec{u})N, \tag{2.4}$$

$$\mathcal{L}_{\pi N}^{(\nu=2)} = \bar{N}\left[\frac{1}{2M}\vec{\nabla}\cdot\vec{\nabla} + 2c_1 m_\pi^2\left(U + U^\dagger\right) + c_2 u_0^2 + c_3(u\cdot u) + i\frac{c_4}{2}\vec{\sigma}\cdot(\vec{u}\times\vec{u})\right]N, \tag{2.5}$$

where N denotes the nucleon field, M is the nucleon mass, D_0 is the gauge-covariant derivative of order zero and $\vec{\sigma}$ are the usual Pauli spin matrices.

Additionally,

$$u_\mu = -\frac{1}{f_\pi}\vec{\tau}\cdot\partial_\mu\vec{\pi} + \cdots \tag{2.6}$$

and

$$U = 1 + \frac{i}{f_\pi}\vec{\tau}\cdot\vec{\pi} + \cdots \tag{2.7}$$

where the $\vec{\tau}$ are the Pauli spin matrices for isospin. The c_i's are the $\pi - N$ low-energy constants (LEC) of order two, which will be given later, and g_A denotes axial-vector coupling constant.

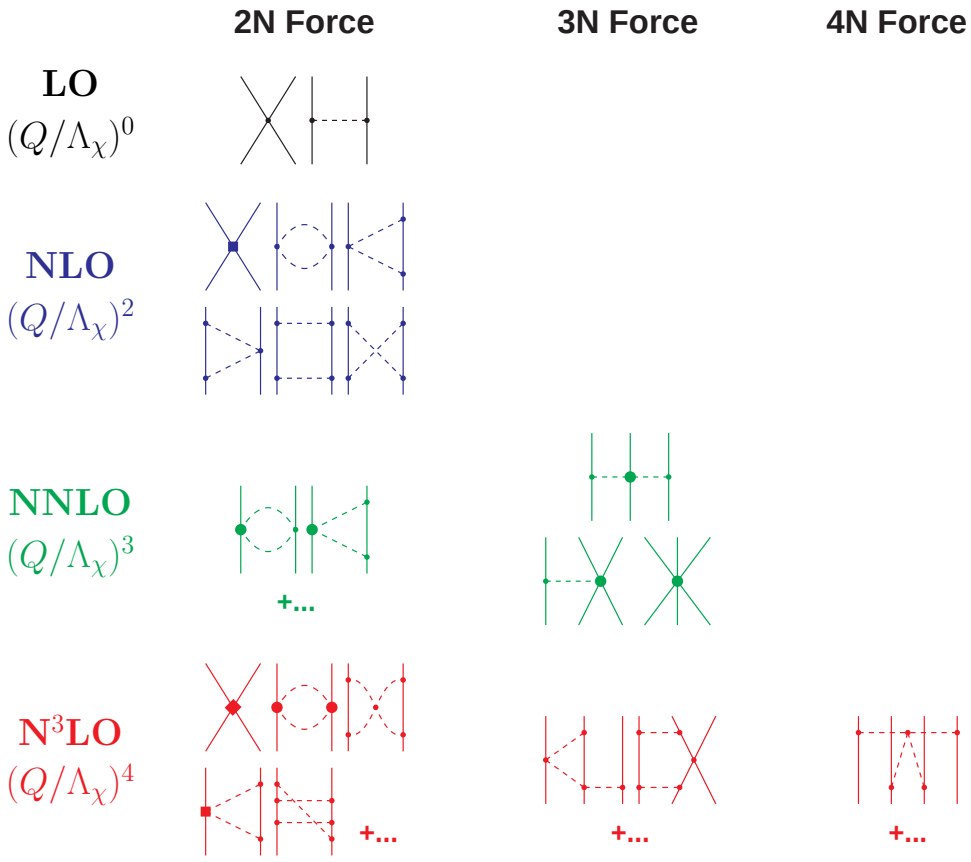

FIGURE 2.1: Feynman diagrams and their related powers. Dashed lines are pions and solid lines are nucleons. The small dots and large dots, solid squares and diamonds denote vertices of index 0, 1, 2 and 4. Reproduced from Ref. [32] with permission.

CHAPTER 3

NN POTENTIAL BASED ON EFT

3.1 GENERAL STRUCTURE OF THE NN POTENTIAL

The NN potential considered has the following general structure:

$$\begin{aligned} U(r) = & V_C(r) + \vec{\tau}_1 \cdot \vec{\tau}_2 W_C(r) \\ & + \left[V_S(r) + \vec{\tau}_1 \cdot \vec{\tau}_2 W_S(r)\right] \vec{\sigma}_1 \cdot \vec{\sigma}_2 \\ & + \left[V_T(r) + \vec{\tau}_1 \cdot \vec{\tau}_2 W_T(r)\right] S_{12} \\ & + \left[V_{LS}(r) + \vec{\tau}_1 \cdot \vec{\tau}_2 W_{LS}(r)\right] \vec{L} \cdot \vec{S} \end{aligned} \tag{3.1}$$

Where V_α's are the isoscalar potentials and W_α's are the isovector potentials. S_{12} is the tensor operator, $\vec{L}$ is the orbital angular momentum operator, and $\vec{S}$ is the total spin. The subscripts C,S,T and LS refer to the central, spin-spin, tensor and spin-orbit contributions. r is the distance to a nucleon.

The potentials in the following sections are usually first derived in momentum space and then subjected to a Fourier transformation into configuration space. See Ref. [33] for details.

3.2 PION EXCHANGE

3.2.1 *One-pion exchange at LO*

The leading order (LO), also called the lowest order ($\nu = 0$), is the static one pion exchange (1PE) between nucleons. It takes on the following form in position space [33]:

$$W_S^{(\nu=0)}(r) = \frac{g_A^2 m_\pi^2}{48\pi f_\pi^2} \frac{e^{-x}}{r} \tag{3.2}$$

$$W_T^{(\nu=0)}(r) = \frac{g_A^2}{48\pi f_\pi^2} \frac{e^{-x}}{r^3}(3 + 3x + x^2) \tag{3.3}$$

with x being $m_\pi r$. The 1PE is singular as $r \to 0$ and thus must be regularized. For this purpose one multiplies equations 3.2 and 3.3 with the regulator function

$$f_{1PE}\,(n, R_0; r) = 1 - \exp\left(-\left(\frac{r}{R_0}\right)^{2n}\right) \tag{3.4}$$

which suppressed the potential at short distances. We use $n = 2$ and will discuss the choices for R_0 below.

3.2.2 *Two-pion exchange at NLO*

At next-to-leading order (NLO), the first two pion exchange contribution occurs. The Feynman diagrams for this are the second row, first column of figure 2.1. In configura-

tion space, they are given by [33]:

$$W_C^{(2)} = \frac{m_\pi}{128\pi^3 f_\pi^4}\frac{1}{r^4}\Big\{\Big[1+2g_A^2(5+2x^2)-g_A^4(23+12x^2)\Big]K_1(2x) + x\Big[1+10g_A^2-g_A^4(23+4x^2)\Big]K_0(2x)\Big\} \tag{3.5}$$

$$V_S^{(2)} = \frac{g_A^4 m_\pi}{32\pi^3 f_\pi^4}\frac{1}{r^4}\Big[3xK_0(2x)+(3+2x^2)K_1(2x)\Big] \tag{3.6}$$

$$V_T^{(2)} = \frac{g_A^4 m_\pi}{128\pi^3 f_\pi^4}\frac{1}{r^4}\Big[-12xK_0(2x)-(15+4x^2)K_1(2x)\Big] \tag{3.7}$$

where K_0 and K_1 are the modified Bessel functions.

3.2.3 *Two-pion exchange at N^{2}LO*

At next-to-next-to-leading order ($\mathrm{N^2LO}$), the 2PE contribution is given by:

$$V_C^{(3)} = \frac{3g_A^2}{32\pi^2 f_\pi^4}\frac{e^{-2x}}{r^6}\Big[2c_1x^2(1+x)^2+c_3(6+12x+10x^2+4x^3+x^4)\Big] \tag{3.8}$$

$$W_S^{(3)} = \frac{g_A^2}{48\pi^2 f_\pi^4}\frac{e^{-2x}}{r^6}c_4(1+x)(3+3x+2x^2) \tag{3.9}$$

$$W_T^{(3)} = \frac{-g_A^2}{48\pi^2 f_\pi^4}\frac{e^{-2x}}{r^6}c_4(1+x)(3+3x+x^2) \tag{3.10}$$

To regularize the 2PE potentials as r is now to the sixth power, we multiply them by

$$f_{2PE}(n,R_0;r) = \left[1-\exp\left(-\left(\frac{r}{R_0}\right)^2\right)\right]^n \tag{3.11}$$

with $n=4$.

3.3 CONTACT POTENTIALS

Contact terms are used in chiral perturbation theory to describe short range interactions. They are depicted in figure 2.1 as crossed solid lines. This section gives the terms for $\nu = 0$ and $\nu = 2$ in the power counting. Note that contact terms appear only for even values of ν [32].

3.3.1 *Contact interactions at LO*

The most general set of contact interactions that occurs at LO ($\nu = 0$) is given by [36]

$$V_{cont}^{(0)} = \left[\alpha_1 + \alpha_2 \vec{\sigma}_1 \cdot \vec{\sigma}_2 + \alpha_3 \vec{\tau}_1 \cdot \vec{\tau}_2 + \alpha_4 \vec{\sigma}_1 \cdot \vec{\sigma}_2 \vec{\tau}_1 \cdot \vec{\tau}_2\right] f^{(0)}\left(n, R_0; r\right) \tag{3.12}$$

where $f^{(0)}\left(n, R_0; r\right)$ is the regulator function. With $n = 2$, this is given by

$$f^{(0)}\left(2, R_0; r\right) = \frac{\hbar c}{\pi \Gamma\left(\frac{3}{4}\right) R_0^3} e^{-\left(\frac{r}{R_0}\right)^4} \tag{3.13}$$

Equation 3.12 can be rewritten as

$$\begin{aligned} V_{cont}^{(0)} = \frac{1}{16}\Big\{ & a_{00}\left(1 - \vec{\sigma}_1 \cdot \vec{\sigma}_2\right)\left(1 - \vec{\tau}_1 \cdot \vec{\tau}_2\right) \\ & + a_{01}\left(1 - \vec{\sigma}_1 \cdot \vec{\sigma}_2\right)\left(3 + \vec{\tau}_1 \cdot \vec{\tau}_2\right) \\ & + a_{10}\left(3 + \vec{\sigma}_1 \cdot \vec{\sigma}_2\right)\left(1 - \vec{\tau}_1 \cdot \vec{\tau}_2\right) \\ & + a_{11}\left(3 + \vec{\sigma}_1 \cdot \vec{\sigma}_2\right)\left(3 + \vec{\tau}_1 \cdot \vec{\tau}_2\right)\Big\} f^{(0)}\left(2, R_0; r\right), \end{aligned} \tag{3.14}$$

where the coefficients are a_{ST} with S being the total spin and T the total iso-spin of the two nucleon system. The α_i coefficients used in 3.12 and the a_{ST} coefficients used in 3.14 are related to each other by

$$\begin{aligned}
\alpha_1 =& \frac{1}{16}\left(a_{00} + 3a_{01} + 3a_{10} + 9a_{11}\right) \\
\alpha_2 =& \frac{1}{16}\left(-a_{00} - 3a_{01} + a_{10} + 3a_{11}\right) \\
\alpha_3 =& \frac{1}{16}\left(-a_{00} + a_{01} - 3a_{10} + 3a_{11}\right) \\
\alpha_4 =& \frac{1}{16}\left(a_{00} - a_{01} - a_{10} + a_{11}\right)
\end{aligned} \tag{3.15}$$

For fitting purposes [32], eq. 3.14 is more convenient, because it projects the contact terms on precise spin-isospin states.

3.3.2 *Contact interactions at NLO*

The set of NLO contact interactions that we use is given by

$$\begin{aligned}
V_{cont}^{(2)} =& \left[\beta_1 + \beta_2 \vec{\sigma}_1 \cdot \vec{\sigma}_2 + \beta_3 \vec{\tau}_1 \cdot \vec{\tau}_2 + \beta_4 \vec{\sigma}_1 \cdot \vec{\sigma}_2 \vec{\tau}_1 \cdot \vec{\tau}_2\right] Q^2 f_{qq}^{(2)}\left(n, R_0; r\right) \\
&+ b_{LS,1} \frac{\left(3 + \vec{\tau}_1 \cdot \vec{\tau}_2\right)}{4} \vec{L} \cdot \vec{S}\, f_{LS}^{(2)}\left(n, R_0; r\right) \\
&+ \left(\beta_6 + \beta_7 \vec{\tau}_1 \cdot \vec{\tau}_2\right) S_{12}\, f_T^{(2)}(n, R_0; r)
\end{aligned} \tag{3.16}$$

where the regulator functions for $n = 2$ are used, which are given by

$$f_{qq}^{(2)}(2, R_0; r) = \frac{4r^2}{R_0^4}\left[5 - 4\left(\frac{r}{R_0}\right)^4\right] f^{(0)}(2, R_0; r) \tag{3.17}$$

$$f_{LS}^{(2)}(2, R_0; r) = \frac{4}{R_0^4}\left(\frac{r}{R_0}\right)^2 f^{(0)}(2, R_0; r) \tag{3.18}$$

$$f_{T}^{(2)}(2, R_0; r) = \frac{8r^2}{3R_0^4}\left[1 - 2\left(\frac{r}{R_0}\right)^4\right] f^{(0)}(2, R_0; r) \tag{3.19}$$

Similar to the LO contacts (Eq. 3.14), the β_i's ($i = 1, \cdots, 4$) are rearranged with four projection operators with coefficients b_{ST}. Moreover,

$$(\beta_6 + \beta_7 \vec{\tau}_1 \cdot \vec{\tau}_2) = \frac{b_{T,0}\,(1 - \vec{\tau}_1 \cdot \vec{\tau}_2)}{4} + \frac{b_{T,1}\,(3 + \vec{\tau}_1 \cdot \vec{\tau}_2)}{4} \tag{3.20}$$

implying

$$\beta_6 = \frac{1}{4}\,(b_{T,0} + 3b_{T,1}) \tag{3.21}$$

$$\beta_7 = \frac{1}{4}\,(b_{T,1} - b_{T,0}) \tag{3.22}$$

CHAPTER 4

RESULTS

4.1 PHASE SHIFTS FOR NUCLEON-NUCLEON SCATTERING

Presented here are the results for the phase shifts up to $T_{lab} = 250$ MeV. The phase shifts are calculated from the potentials. As explained in the previous section, the various contributions to the potential are regularized with a cut-off radius R_0. Three cut-off radii were checked for the fitting process. Table 4.1 contains the values used in the fitting process as well as the LECs used. The phase shifts are shown in Figure 4.1. The phase shifts are a displacement of the partial waves of low angular momentum, denoted by ${}^{2s+1}L_j$ where s is the total spin, L is the orbital angular momentum (written as $S, P, D, F, ...$ for when $L = 0, 1, 2, 3, ...$) and j is the total angular momentum. Table 4.2 contains parameters for fitting the potentials to the experimental data for each cut-off. Table 4.3 gives the scattering lengths and effective ranges for each cut-off as well as the deuteron properties. Table 4.4 contains χ^2 per datum for the fits for each cut-off. This compares how well the fitted potentials are to experimental data and compares them to χ^2 per datum of work from another work.

4.1.1 *S-Waves*

Table 4.3 gives the scattering lengths and effective ranges for ${}^1S_0$ and ${}^3S_0$. Fig. 4.1 shows the phase shifts. The *S*-waves are in sufficient agreement with the experimental data.

4.1.2 *P-Waves*

There are four *P*-waves. Their phase shifts are in agreement with experimental data.

4.1.3 *D-Waves*

The ${}^3D_1$ phase shift is in agreement with experimental data, but the ${}^1D_2$, ${}^3D_2$ and ${}^3D_3$ phase shifts are high due to lack of contact parameters that do not exist at N^{2}LO.

4.1.4 *F-Waves*

${}^3F_2$ phase shift matches well for 1.0 fm cut-off, but is high for the 0.9 fm cut-off and too low for the 1.1 fm cut-off. ${}^1F_3$ and ${}^3F_3$ phases match well with the data.

4.1.5 *Mixing Parameters*

The tensor operator mixes two partial waves of equal parity. The mixing parameter shows how mixed the partial waves are. ϵ_1 falls below the experimental data but ϵ_2 and ϵ_3 match the experimental data.

4.2 THE DEUTERON

Table 4.3 gives important deuteron properties as predicted by the cut-offs. B_d is the Deuteron binding energy, A_s is the asymptotic S state, η is the asymptotic D/S state, Q is the quadrupole moment and P_D is the D-state probability. The predictions are quite close to empirical.

TABLE 4.1: Parameters used in exchange potentials

parameter	potential (unit)	Empirical
M_p	938.2720 (MeV)	938.272046(21) [37]
M_n	939.5653 (MeV)	939.5653(79) [37]
$\bar{M}$	938.9183 (MeV)	
m_{π^0}	134.9766 (MeV)	134.9766 [37]
$m_{\pi^\pm}$	139.5702 (MeV)	139.57018 [37]
g_A	1.29	1.2759(45) [37]
f_π	92.4 (MeV)	92.2 ± 0.2 [37]
c_1	-0.58 (GeV^{-1})	-0.58 [38]
c_3	-3.14 (GeV^{-1})	-3.14 [38]
c_4	2.19 (GeV^{-1})	2.19 [38]

TABLE 4.2: Contact term parameters for the different cut-off fits

	cut-off R_0		
parameters	0.9 fm	1.0 fm	1.1 fm
a_{00}	8.10	5.5	4.575
a_{01}	2.7331	0.83427	-0.44
a_{10}	2.3585	0.60885259	-0.7622
a_{11}	6.12	3.69	2.50
b_{00}	-0.11	-0.11	-0.11
b_{01}	0.145	0.285	0.372
b_{10}	0.10	0.23	0.38
b_{11}	-0.19	-0.09	0.0
$b_{T,0}$	0.0	0.0	0.0
$b_{T,1}$	-0.012	0.0	0.0
$b_{LS,1}$	0.0	-1.11	-1.12

TABLE 4.3: Low-energy parameters and deuteron properties as predicted by the potentials denoted by their cut-off radius R_0. a and r are the scattering lengths and effective ranges in fm.

	0.9 fm	1.0 fm	1.1 fm	Empirical
$^1S_0$				Ref. [32, Table 8]
a^c_{pp}	-7.814	-7.815	-7.814	-7.8149(29)
r^c_{pp}	2.766	2.770	2.767	2.769(14)
a_{np}	-23.738	-23.738	-23.754	-23.740(20)
r_{np}	2.698	2.702	2.698	2.77(5)
$^3S_1$				Ref. [32, Table 8]
a_t	5.396	5.407	5.429	5.419(7)
r_t	1.723	1.739	1.769	1.753(8)
deuteron				Ref. [32, Table 9]
B_d (MeV)	2.224579	2.224575	2.224580	2.224575(9)
A_s (fm$^{-1/2}$)	0.8801	0.8824	0.8867	0.8846(9)
η	0.0255	0.0253	0.0250	0.0256(4)
Q (fm^2)	0.275	0.273	0.271	0.2859(3)
P_D (%)	5.59	5.21	4.77	

TABLE 4.4: χ^2 per datum for various fits using different cut-off radii R_0 and a potential from Ref. [36] with R_0 = 1.0 fm.

T_{lab} bins (MeV)	# of data	cut-off R_0			
		0.9 fm	1.0 fm	1.1 fm	Ref. [36] at 1.0 fm
np					
0 - 100	1124	1.43	1.60	2.02	1.41
0 - 190	1570	1.63	1.85	2.40	2.60
pp					
0 - 100	776	1.63	1.85	2.30	3.13
0 - 190	1187	5.41	6.66	9.98	9.41

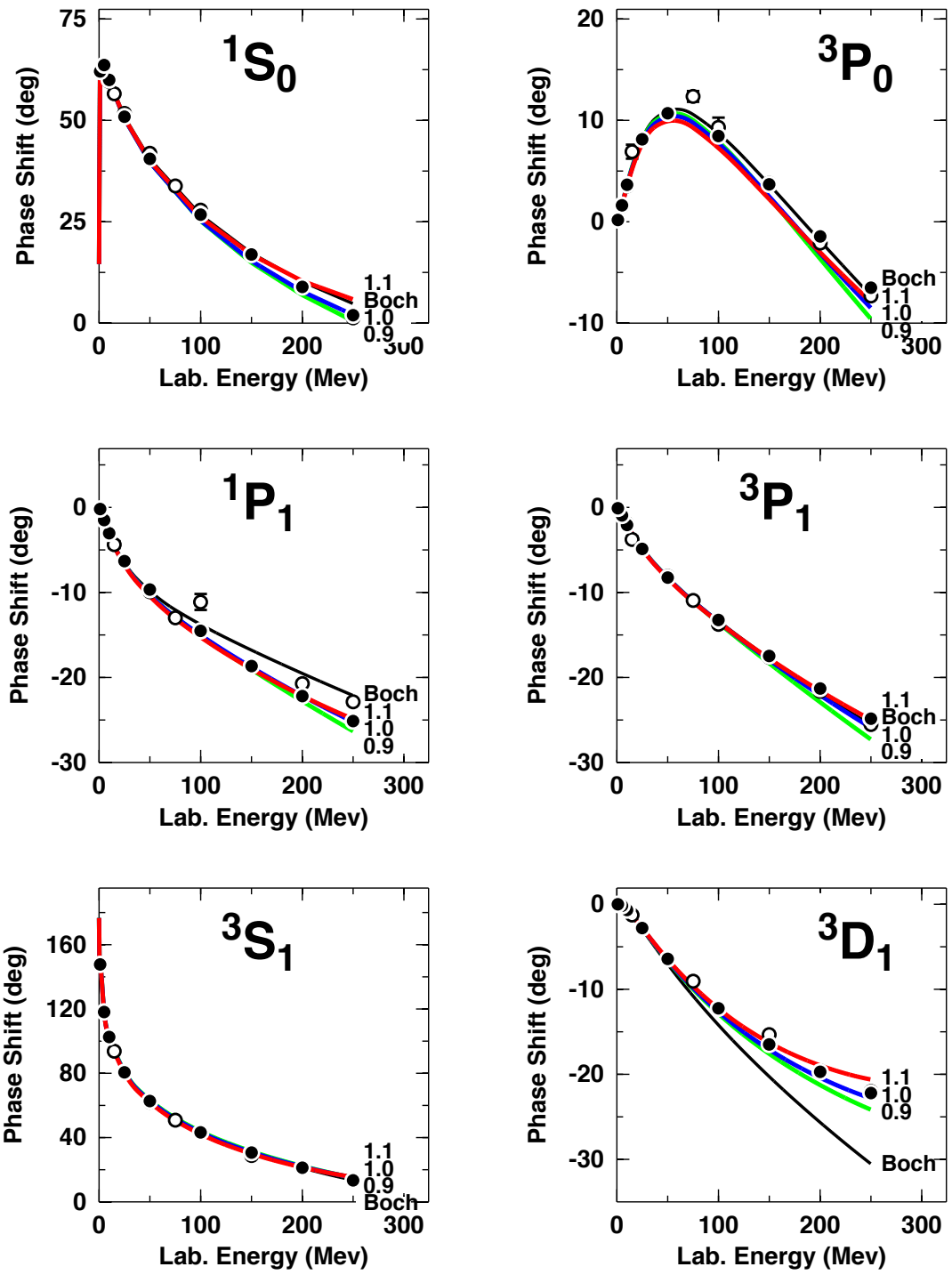

FIGURE 4.1: Phase shifts and mixing parameters. The red, blue and green lines are the predictions by the potentials with cut-off radius R_0 = 1.1, 1.0 and 0.9 fm, respectively. The black line is the potential of Ref. [36] with R_0 = 1.0 fm. The solid dots are the Nijmegen multienergy *np* phase shift analysis [39]. The open circles are the VPI/GWU single-energy *np* analysis SM07 [40].

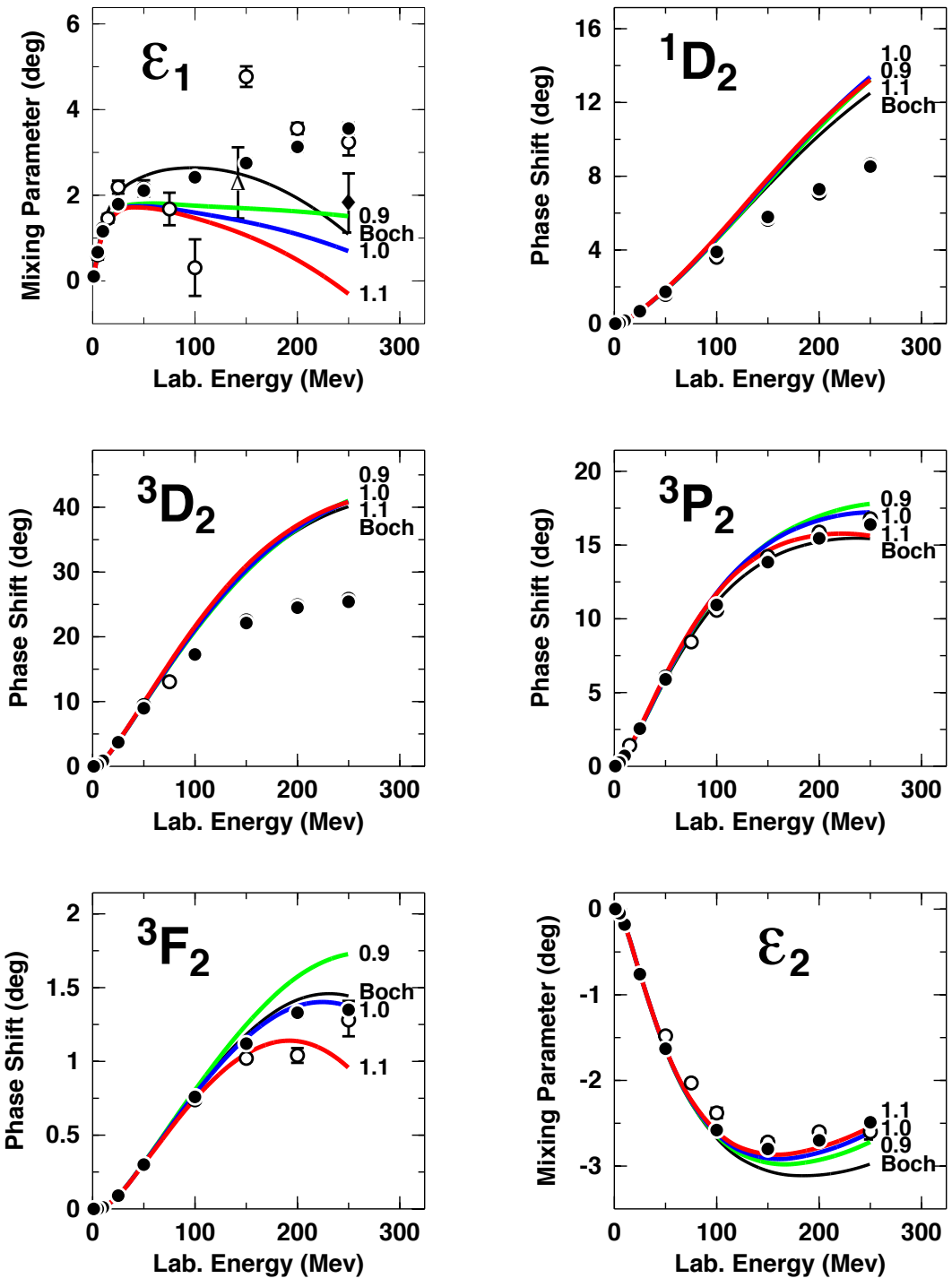

Fig. 4.1 continued

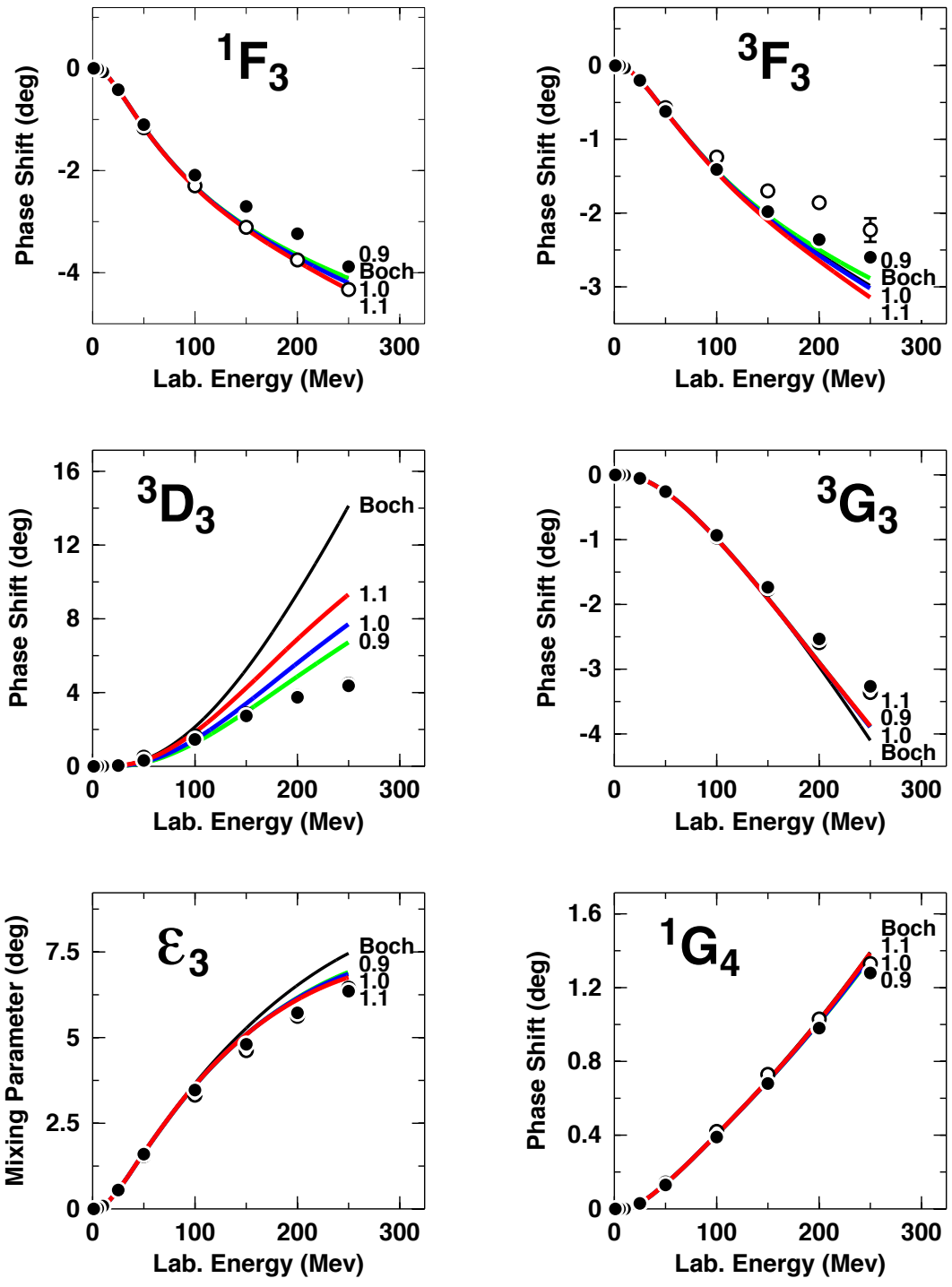

Fig. 4.1 continued

CHAPTER 5

CONCLUSION

In this thesis, I have applied chiral effective field theory up to N^{2}LO to construct local NN potentials in configuration space. Because of the singular nature of the one- and two- pion exchange potentials at short distances, a regulator function is applied to the pion-exchange potentials to suppresses the potential as $r \to 0$. The parameter of this regulator, R_0, is varied from 0.9 fm to 1.1 fm.

Moreover, contact potentials are introduced to parametrize the NN potential at short range. We use four contact terms at LO and seven terms at N^{2}LO. These contributions are "smeared out" due to the use of cut-off functions that depend on the above mentioned R_0. The parameters of these 11 contact terms are essentially free and used to fit the partial waves of low angular momentum (the S and P waves).

The reproduction of the phase shifts of the S, P and F waves is very good. However, there are problems with some of the D waves ($^1D_2$ and $^3D_2$). The χ^2 per datum of the reproduction of the NN data is, in general, below 2.0 for the interval 0-100 MeV, which is satisfactory as it is better than previous work. The description of the np data up to 190 MeV is also acceptable; while for pp, large χ^2 occur above 100 MeV due to some very accurate differential cross section measurements. The deuteron properties are reproduced well.

Over-all our NN potential is more accurate than similar potentials constructed by other researchers, as the chi^2 per datum is smaller than that produced by Ref. [36]. Because of the precision of our position-space potential, it represents a reliable starting

point for microscopic nuclear structure calculations (I.E. ground states of light nuclei) that require a local potential.

BIBLIOGRAPHY

[1] E. Rutherford, Phil. Mag. **21**, 669 (1911).

[2] J. J. Thomson, *Rays of Positive Electricity* (Longmans Green New York, 1913).

[3] R. Machleidt, Adv. Nucl. Phys. **19**, 189 (1989).

[4] J. Chadwick, Proc. Roy. Soc. (London) **A136**, 692 (1932).

[5] E. Winger, Phys. Rev. **43**, 252 (1933).

[6] E. Majorana, Z. Physik **82**, 137 (1933).

[7] W. Heisenberg, Z. Physik **77**, 1 (1932).

[8] M. Tuve, N. Heydenburg, and L. Hafstad, Phys. Rev. **50**, 806 (1936).

[9] J. Chadwick and M. Goldhaber, Nature **134**, 237 (1934).

[10] H. Yukawa, Proc. Phys. Math. Soc. (Japan) **17**, 48 (1935).

[11] A. Proca, J. Phys. Radium **7**, 347 (1936).

[12] N. Kemmer, Proc. Roy. Soc. **A166**, 127 (1936).

[13] J. Schwinger, Phys. Rev. **61**, 387 (1942).

[14] C. Møller and L. Rosenfeld, Math.-Fys. Medd. **17** (1940).

[15] W. Pauli, *Meson Theory of Nuclear Forces* (Interscience, New York, 1946).

[16] C. M. C. Lattes, H. Muirhead, G. P. S. Occhialini, and C. F. Powell, Nature **159**, 694 (1947).

[17] M. Taketani, S. Nakamura, and M. Sasaki, Prog. Theor. Phys. (Kyoto) **6**, 581 (1951).

[18] K. A. Brueckner and K. M. Watson, Phys. Rev. **90**, 699 (1953).

[19] K. A. Brueckner, M. Gell-Mann, and M. Goldberger, Phys. Rev. **90**, 476 (1953).

[20] M. Gellman and M. Levy, Nuovo Cimento **16**, 705 (1960).

[21] S. Weinberg, Phys. Rev. Lett. **18**, 188 (1967).

[22] G. E. Brown, *Mesons in Nuclei*, Vol. 1 (North-Holland, Amsterdam, 1979) p. 330.

[23] A. D. Jackson, D. O. Riska, and B. Verwest, Nucl. Phys. **A249**, 397 (1975).

[24] M. Lacombe, B. Loiseau, J. M. Richard, R. V. Mau, J. Côté, P. Pirès, and R. de Tourreil, Phys. Rev. **C21**, 861 (1980).

[25] M. H. Partovi and E. L. Lomon, Phys. Rev. **D2**, 1999 (1970).

[26] M. H. Partovi and E. L. Lomon, Phys. Rev. **D5**, 1192 (1972).

[27] R. Machleidt, K. Holinde, and C. Elster, Phys. Rep. **149**, 1 (1987).

[28] N. Isgur and K. Maltman, Phys. Rev. **D29**, 952 (1984).

[29] S. Weinberg, Physica **96A**, 327 (1979).

[30] E. Epelbaum, W. Glöckle, and U.-G. Meißner, Nucl. Phys. **A637**, 107 (1998).

[31] D. R. Entem and R. Machleidt, Phys. Rev. **C68**, 41001 (2003).

[32] R. Machleidt and D. R. Entem, Phys. Rep. **503**, 1 (2011).

[33] N. Kaiser, R. Brockmann, and W. Weise, Nucl. Phys. **A625**, 758 (1997).

[34] E. Jenkins and A. V. Manohar, Phys. Lett. **B255**, 558 (1991).

[35] H. Shimoyama, *Chiral Symmetry and the Nucleon-Nucleon Interaction: Developing a Chiral NN Potential in Configuration Space*, Ph.D. thesis, University of Idaho (2005).

[36] A. Gezerlis, I. Tews, E. Epelbaum, M. Freunek, S. Gandolfi, K. Hebeler, A. Nogga, and A. Schwenk, Phys. Rev. C **90**, 054323 (2014).

[37] J. Beringer *et al.* (Particle Data Group), Phys. Rev. D **86**, 010001 (2012).

[38] H. Krebs, A. Gasparyan, and E. Epelbaum, Phys. Rev. C **85**, 054006 (2012).

[39] V. G. J. Stoks, R. A. M. Klomp, M. C. M. Rentmeester, and J. J. de Swart, Phys. Rev. **C48**, 792 (1993).

[40] R. L. Arndt, I. I. Strakowsky, and R. L. Workman, Scattering Analysis Interactive Dial-in computer facility (SAID), VPI/GWU, solution SM07 (2007).